Energy 183 (2019) 573–583

Contents lists available at ScienceDirect

Energy

journal homepage: www.elsevier.com/locate/energy

Dynamic performance analysis and optimization of dish solar Stirling engine based on a modified theoretical model

Xiaotian Lai, Minjie Yu, Rui Long*, Zhichun Liu, Wei Liu**

School of Energy and Power Engineering, Huazhong University of Science and Technology, 1037 Luoyu Road, Wuhan, 430074, China

ARTICLE INFO

Article history:
Received 8 January 2019
Received in revised form
9 May 2019
Accepted 20 June 2019
Available online 20 June 2019

Keywords:
Theoretical analysis
Solar thermal utilization
Dish solar Stirling engine

ABSTRACT

A modified theoretical model of dish solar Stirling engine was developed based on a Stirling cycle operating with finite shaft rotating speed and the energy balance equations at hot and cold ends. The convergence of solar receiver temperature and charged gas heat releasing temperature represent the stabilization of solar receiver and Stirling engine respectively, thus, to guarantee a steady operation of the overall system. Impacts of meteorological condition, operational parameter of Stirling engine on system performance were investigated and analyzed systematically. Results indicate that higher solar flux intensity improves system performance while wind deteriorates the system performance. With the input solar energy specified, optimal charged gas mass in Stirling engine exists corresponding to the maximal power output. More effective heater, regenerator and cooler contribute to better optimal system performance. Meanwhile, the charged gas mass optimized under the daily average solar flux intensity achieves the maximal mechanical work in a day with less computation. The maximal theoretical peak power output of 25 kW and overall efficiency of 44% are obtained as high performance heat exchangers are adopted and charged gas mass is optimized.

1. Introduction

Continuous consumption of limited fossil fuels and the appearance of urgent environmental pollution such as greenhouse effect call for the rapid development of green and sustainable energy utilization technology [1]. Solar energy which is of huge amount and completely green, attracts numerous researchers to exploit appropriate methods for the realization of clean and highly effective solar energy utilization such as photovoltaic device [2], solar powered heat engine [3] and absorption chiller [4], solar desalination [5] and solid oxide electrolyzer [6]. Dish solar SE (Stirling engine) is one of the feasible solutions to convert solar energy into electricity and has been successfully constructed and operated in some countries [7]. Dish solar SE is a Stirling engine based solar thermal device. With the advantages of high thermal efficiency [8], variability of heat source [9] and power capacity [10], SE has been investigated numerously with different point views in the recent decades such as the inside flow characters [11] and its potential for hybridizing [12]. Heated by the solar receiver at which concentrated sunshine is converted into thermal energy, dish solar SE is capable to achieve high solar-electrical energy conversion efficiency which is reported as high as 30% in Ref. [13]. For further improving the performance and clarifying more precise physical mechanism in solar SE, some research work in the means of experiment [14] and mathematical modelling [15] were conducted as well.

Fatih Aksoy et al. experimentally investigated and compared the performance of different solar SE cavities manufactured with aluminum, copper and stainless steel. Results indicate aluminum achieves the highest power output and efficiency of 64.4 W and 5.64% but is limited by its low melting point [14]. In their another research, halogen lamps were utilized as the solar source for heating a beta type SE. The experiments were conducted under different lamp power of 400 and 1000 W, results indicate maximum power of 37.08 W and thermal efficiency of 9.27% were achieved with 400 W lamp power. As increasing the lamp power to 1000 W, maximum power and efficiency are both enhanced to 127.17 W and 12.85% respectively [16]. Ana C. Ferreira et al. modeled the concentrator and receiver with a more precise description of energy conservation in receiver to investigate the economic and thermal performance of solar module. The rim angle, dish diameter and receiver diameter were optimized simultaneously with the SQP

* Corresponding author.
** Corresponding author.
E-mail addresses: r_long@hust.edu.cn (R. Long), w_liu@hust.edu.cn (W. Liu).

https://doi.org/10.1016/j.energy.2019.06.131
0360-5442/

(sequential quadratic programming) method. Efficiency of 64% and receiver temperature of 833 K were achieved under the optimal condition [17]. By further coupling this solar model with the adiabatic model of SE, the thermodynamic, economic analysis and optimization of dish solar SE cogeneration system was studied as well [18,19]. The results indicate a thermal power of 11.06 kW and electrical power of 3.65 kW can be achieved with an annual worth of 627 €/year. In addition, their work also indicates the model modification which considers the variance of input solar flux is required to state a more precise analysis of dish solar SE.

For giving guidelines to achieve the optimal system performance, tremendous fundamental theoretical work of dish solar SE has been conducted as well. V. Badescu et al. studied the performance of solar Stirling and Ericsson heat engines. Receiver temperature was optimized analytically for deriving the maximal power output. Results indicate that concentration ratio influences the maximal efficiency of solar-mechanical energy conversion drastically [20]. David A. Blank et al. analyzed the optimal performance of an extraterrestrial solar SE. With the external heat transfer process being considered as thermal radiation, the temperatures of external thermal source and sink were considered constant. The formulation of power output in the form of temperatures of substance and thermal reservoirs was derived and optimized. Results indicate that power output increases with the improvement of heat transfer ability at hot end [21]. S.C. Kaushik et al. modeled an endoreversible Stirling cycle coupled with finite heat capacitive source and sink, by adopting finite time thermodynamic method. Analytical derivation and numerical results were presented. The results indicate that higher temperature of heat source, better effectiveness of heat exchangers are beneficial for improving system performance [22]. Jincan Chen et al. investigated the efficiency bound of a solar powered SE in which heat source and sink both operate with constant temperature. Maximal energy efficiency exits as a function of receiver temperature. Besides, the maximal efficiency and corresponding receiver temperature were derived analytically as well [23]. Tianjun Liao et al. optimized the receiver temperature with Lagrange multiplier method. In addition, they found better system performance can be achieved with less heat leakage [24]. Mohammad Hossein Ahmadi et al. conducted series of multi-objective optimization work to achieve the optimal compromise between the power output, thermal efficiency, entropy generation and entransy loss with NSGA-II (non-dominated sorted genetic algorithm-II) and different decision makers including LINMAP (linear programming techniques for multidimensional analysis of preference), TOPSIS (technique for order preference by similarity to an ideal solution) and Fuzzy. Receiver temperature, substance heat absorbing temperature and heat releasing temperature were optimized to achieve the trade-off among different optimization targets. LINMAP behaves with the minimum deviation with the ideal solution [25–27]. Yaqi Li et al. modeled a theoretical dish solar SE considering that substance exchanges heat with heat source and sink which has infinite heat capacity. Analytical solution for two special cases were derived to obtain the maximal power output, and optimal theoretical thermal efficiency of 34% was obtained [28].

Within the previous valuable theoretical work of dish solar SE, the temperature of solar receiver was always treated as an independent variable and optimized though it depends on the energy balance of supplement of upstream, requirement of downstream and the local dissipation. M. Costea et al. noticed the energy balance of supplement and requirement at hot end, and modeled the solar Stirling engine considering the finite rotation speed of SE shaft. Optimization work was conducted with Lagrange undetermined multipliers method and the results indicate that the real efficiency is around half of the ideal cycle while the engine operates with maximal power output [29].

In order to model the theoretical dish solar SE as a function of more direct influential parameters (such as the solar flux intensity, wind velocity, and charged gas mass of SE), the energy balance of supplement, transfer and requirement at hot and cold ends were considered simultaneously. The corresponding algorithm and case study were stated to illustrate a precise insight of this modified theoretical model. Furthermore, the sensitivity analysis was conducted to investigate the influence of meteorological condition and operational parameters of SE on the system performance. Maximal power output under different heat transfer ability of heater, regenerator and cooler were obtained and compared. Finally, in order to achieve the daily maximal generatable work, the corresponding optimization strategy was discussed and the daily dynamic theoretical performance was obtained as well.

2. Theoretical model and algorithm

2.1. Theoretical model

Dish solar Stirling engine system mainly consists of three components: concentrator for focusing the sunshine on receiver with high flux intensity, receiver for converting the solar energy into thermal energy and heating the charged gas in SE, and Stirling engine module for generating shaft power with the heat supplement from receiver. For the incident solar flux intensity fluctuates significantly with time in a day, the dynamic power output of dish solar SE is hard for direct utilization and normally stored for the sequential stable releasing. The corresponding thermally irreversible model of dish solar SE can be described as the theoretical Stirling cycle coupled with a heat source having stable temperature and coolant having finite thermal capacity as Fig. 1 depicts. Meanwhile, the imperfect regeneration originated from the essential temperature difference for heat transfer in regenerator is considered as well. The relative governing equations are stated below.

Considering some optical losses such as imperfect reflection of the parabolic surface and the optical interception at the entrance of receiver, an optical efficiency is multiplied with the first term in Eq. (1) to express the solar energy arriving at receiver. Meanwhile, T_H (receiver temperature) drives partial heat to environment in the form of convection and radiation. Hence, the thermal energy utilizable for SE can be expressed as Eq. (1) [30].

$$\dot{Q}_{H,Supplement} = IA_R C\eta_{optical} - h_c A_R (T_H - T_0) - \varepsilon\sigma A_R \left(T_H^4 - T_{sky}^4\right) \tag{1}$$

where $h_c = 5.7 + 3.8V_{wind}$ and $T_{sky} = 0.0552T_0^{1.5}$ are the convective heat transfer coefficient and sky temperature [30]. The thermal energy obtained by receiver then transfers through the hot end heat exchanger with heat transfer ability of K_H (production of heat transfer coefficient and area) to heat the charged gas as Eq. (2).

$$\dot{Q}_{H,Transfer} = K_H(T_H - T_h) \tag{2}$$

Meanwhile, the heat absorbing requirement of SE depends on the operational condition. Two heat absorbing processes of isochoric process 2–3 (Eq. (3)) and isothermal process 3–4 (Eq. (4)) absorb heat from the regenerator matrix and external heat source respectively [28]. However, as the realistic regenerator is imperfect, regeneration loss is supplied by the external heat source.

$$Q_{23} = mc_v(T_h - T_l) \tag{3}$$

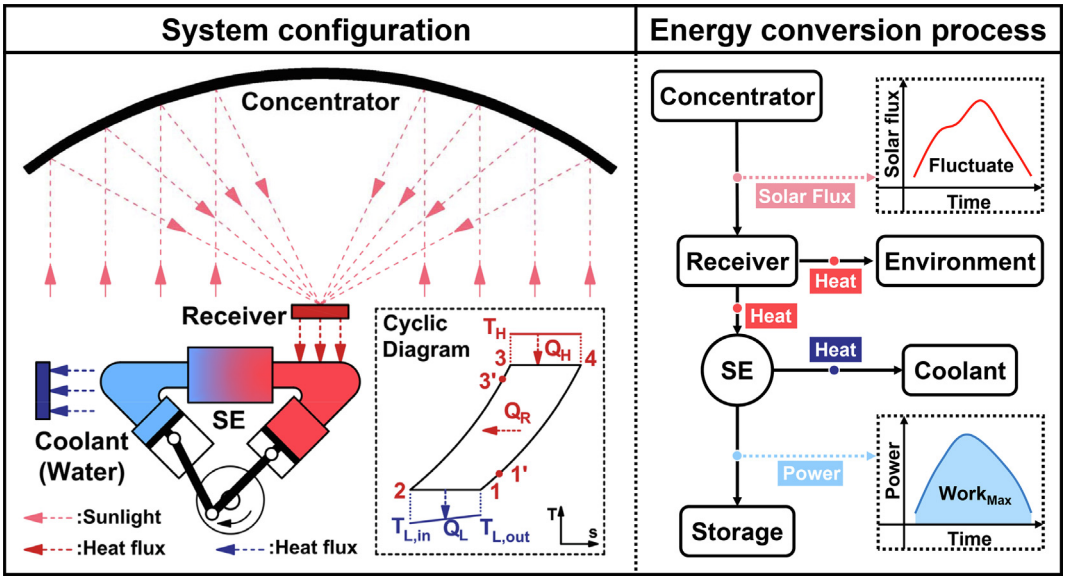

Fig. 1. System configuration and energy conversion process diagram.

$$Q_{34} = \int_{v_3}^{v_4} mpdv = \int_{v_3}^{v_4} \frac{mR_gT_h}{v} dv = mR_gT_h \ln\left(\frac{v_4}{v_3}\right) \tag{4}$$

Hence, the cyclic heat absorbing requirement from solar receiver can be expressed as Eq. (5).

$$Q_H = Q_{3'3} + Q_{34} = mc_v(T_h - T_l)(1-\varepsilon_R) + mR_gT_h \ln\left(\frac{v_4}{v_3}\right) \tag{5}$$

As the shaft of SE rotates with a frequency of F which means the same amount of thermodynamic cycles are completed per second [31], heat requirement rate from external heat source has Eq. (6).

$$\dot{Q}_{H,Load} = FQ_H = Fmc_v(T_h - T_l)(1-\varepsilon_R) + FmR_gT_h \ln\left(\frac{v_4}{v_3}\right) \tag{6}$$

With no heat leakage considered, the energy balance equation should be met as Eq. (7). Namely, the heat supplied by solar receiver equals to the heat transferred in heat exchanger and the heat required by SE under steady operation condition.

$$\dot{Q}_{H,Supplement} = \dot{Q}_{H,Transfer} = \dot{Q}_{H,Load} \tag{7}$$

As to the cooling system, heat released is designated as minus. When the coolant with finite heat capacity flows through the cooler, temperature increases linearly heated by the compressed gas in SE. Hence, the thermal load undertaken by the coolant is given by Eq. (8).

$$\dot{Q}_{L,Load} = -\dot{m}_w c_{p,w}(T_{L,out} - T_{L,in}) \tag{8}$$

For the temperature of coolant varies in the cooling process, the heat transferred in cooler can be expressed as the production of heat transfer ability and log-mean temperature difference in Eq. (9) [32,33].

$$\dot{Q}_{L,Transfer} = -K_L \frac{(T_l - T_{L,in}) - (T_l - T_{L,out})}{\ln\left(\frac{T_l - T_{L,in}}{T_l - T_{L,out}}\right)} \tag{9}$$

Heat releasing processes of the internal Stirling cycle are isothermal heat releasing to the coolant 1–2 (Eq. (10)) and isochoric heat releasing to the regenerator matrix in 4-1 (Eq. (11)). Imperfect heat regeneration also means more heat released to coolant, the cyclic heat released can be expressed as Eq. (12) [28].

$$Q_{12} = \int_{v_1}^{v_2} mpdv = \int_{v_1}^{v_2} \frac{mR_gT_l}{v} dv = mR_gT_l \ln\left(\frac{v_2}{v_1}\right) \tag{10}$$

$$Q_{41} = mc_v(T_l - T_h) \tag{11}$$

$$Q_L = Q_{1'1} + Q_{12} = mc_v(T_l - T_h)(1-\varepsilon_R) + mR_gT_l \ln\left(\frac{v_2}{v_1}\right) \tag{12}$$

The heat released by charged gas in SE per second can be stated as Eq. (13).

$$\dot{Q}_{L,Supplement} = FQ_L = Fmc_v(T_l - T_h)(1-\varepsilon_R) + FmR_gT_l \ln\left(\frac{v_2}{v_1}\right) \tag{13}$$

Similarly, energy balance equation should be met as Eq. (14) in the cooling process as well.

$$\dot{Q}_{L,Supplement} = \dot{Q}_{L,Transfer} = \dot{Q}_{L,Load} \tag{14}$$

With the energy input and output of each subsystem being obtained, the power output of SE, thermal efficiencies of receiver, SE and the overall system can be expressed as Eq. (15-18).

$$P = F(Q_H - Q_L) = FmR_g(T_h - T_l)\ln\left(\frac{v_4}{v_3}\right) \tag{15}$$

$$\eta_{Receiver} = \frac{\dot{Q}_{H,Load}}{IA_RC\eta_{optical}} \tag{16}$$

$$\eta_{SE} = \frac{P}{\dot{Q}_{H,Load}} \tag{17}$$

$$\eta = \frac{P}{IA_R C} = \eta_{optical}\eta_{Receiver}\eta_{SE} \tag{18}$$

The efficiency of solar receiver in Eq. (16) represents the utilizable heat gained from the sunshine which arrives at receiver. Meanwhile, the engine efficiency indicates the ratio of mechanical power generated from the utilizable solar heat in Eq. (17). For the overall system, the efficiency in Eq. (18) represents the energy conversion ability from the captured solar energy to mechanical power.

2.2. Algorithm

The algorithm flow chart in Fig. 2 illustrates the establishment method of the modified dish solar SE theoretical model. The first three steps initialize the operational and geometrical parameters, then the following steps are set for achieving the steady operation with two level iterations. In the external level iteration (steps 4–13), a hypothetical $T_{H,1}$ is set to calculate $\dot{Q}_{H,Supplement}$ and T_h. Then governed by the specified heat transfer ability of cooler and mass flow rate of coolant under a hypothetical T_h, a corresponding unified T_l exists to reach the energy balance in heat releasing process with the internal level iteration (steps 7–11) according to Eq. (14). $\dot{Q}_{L,Supplement}$, $T_{L,out}$ and $\dot{Q}_{L,Transfer}$ are solved successively with a hypothetical $T_{l,1}$. By checking the energy balance condition with the relative error in Eq. (19) at step 11 and updating a new T_l for step 8 repeatedly, the unified T_l can be solved to meet the energy balance equation Eq. (14). Namely, the SE subsystem operates steadily at step 12. Then the corresponding thermal load $\dot{Q}_{H,Load}$ can be calculated as well. At step 13, checking the energy balance condition of hot end with the relative error in Eq. (20) to testify whether solar receiver operates steadily or not. As the convergence criteria is met, the power output and thermal efficiency under a steady operational condition can be obtained.

3. Results and analysis

3.1. Case study

In order to present a more precise description of the calculation procedure, a case study with the initial values in Table 1 was conducted.

In the case study, helium and water are selected as the substance and coolant in SE respectively. The convergence processes are depicted in Fig. 3. Red dots represent the relative errors between thermal supplement and load in heating process under each iteration step. Under each hypothetical T_H, the internal level iteration for the convergence of T_l is achieved as well which is plotted with the blue dots. Begin with red dot 1 and set $T_{H,1}$ as 1100 K arbitrarily, then the corresponding internal level iteration is plotted in Fig. 3-(1). During the internal level iteration, a hypothetical $T_{l,1}$ is set as 647.64 K. The minus relative error indicates heat transferred through cooler exceeds the heat released from SE according to Eq. (19). Hence T_l is updated degressively until $T_{l,5}$ is set as 319.06 K, $\dot{Q}_{L,Supplement}$ exceeds $\dot{Q}_{L,Transfer}$ at this step. Then an increased $T_{l,6}$ is set and the relative error decreases. By adjusting the upper and lower bounds of T_l continuously, the convergence of internal level iteration is achieved with δ_L less than 1e-5. As SE operates steadily, thermal load of SE is calculated to testify the energy balance condition at hot end. The minus relative error of −24% indicates that $\dot{Q}_{H,Supplement}$ is insufficient to meet the thermal requirement of SE. Namely, the real T_H is less than $T_{H,1}$ to reduce the thermal losses

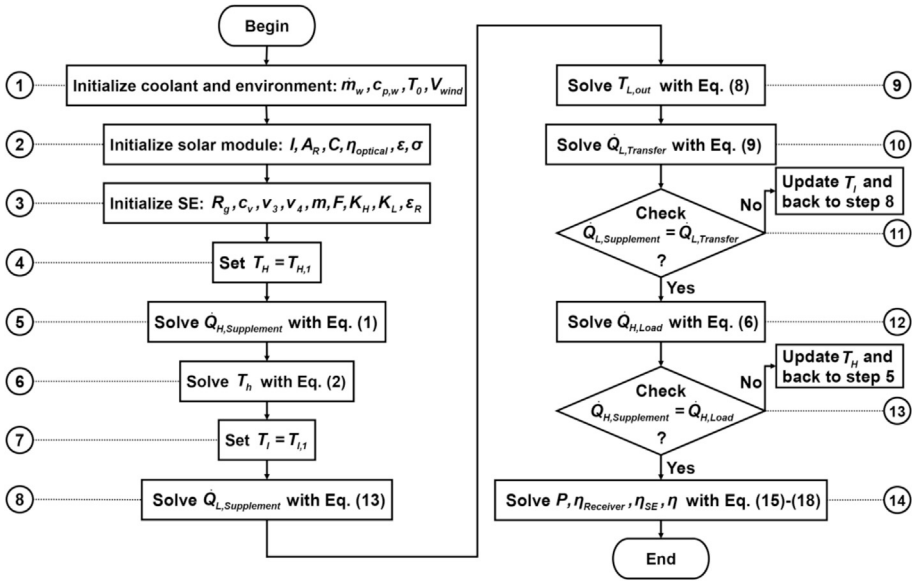

Fig. 2. Algorithm flow chart.

$$\delta_L = \frac{\dot{Q}_{L,Supplement} - \dot{Q}_{L,Transfer}}{\dot{Q}_{L,Transfer}} \tag{19}$$

$$\delta_H = \frac{\dot{Q}_{H,Supplement} - \dot{Q}_{H,Load}}{\dot{Q}_{H,Load}} \tag{20}$$

Table 1
Initialization of case study.

Coolant and environment					
$\dot{m}_w$(kg/s)		$c_{p,w}$(J/(kg·K))		T_0(K)	V_{wind}(m/s)
0.4		4180		293.15	0
Solar thermal module					
I(W/m^2)	A_R(m^2)	C(−)	$\eta_{Optical}$(%)	ε(−)	σ(W/(m^2·K^4))
700	0.0491	1250	80	0.88	5.67e-8
Stirling engine					
Gas	R_g(J/(kg·K))	c_v(J/(kg·K))	v_3(m^3/kg)	v_4(m^3/kg)	
Helium	2077	3116	0.6	1.3	
m(kg)	F(Hz)	K_H(W/K)	K_L(W/K)	ε_R(%)	
8e-4	25	300	500	80	

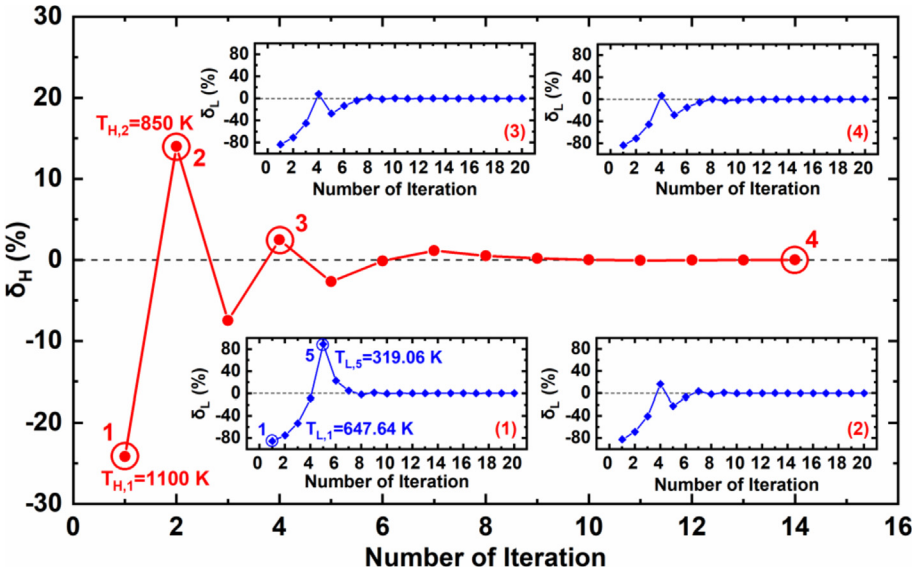

Fig. 3. Convergence of T_l and T_H.

then increase the thermal supplement. A decreased $T_{H,2}$ of 850 K is updated in red dot 2 and the relative error is checked. The same procedures are conducted until a steady T_H is achieved with δ_H less than 1e-5.

When the correct T_H and T_l are found simultaneously, the dish solar SE cycle operates steadily. The corresponding T-s, p-v and energy consumption distribution diagrams were plotted in Fig. 4. In Fig. 4-(a), the charged gas releases heat to coolant isothermally under 331.87 K and drives the temperature of coolant to increase by around 10 K in process 1–2. Then heated by the regenerator matrix and extra heat from solar receiver, the temperature of charged gas increases to 819.25 K via isochoric heating and expands isothermally with stable heat supplement from solar receiver. Finally, majority of the residual heat was transferred to the regenerator matrix and small quantity was released to the coolant due to the imperfect regeneration. With the results of case study in Table 2, the entire solar power input is 42.95 kW. The optical, convective and radiative energy losses are 8.59, 0.18 and 1.80 kW which occupy 20.00%, 0.41% and 4.18% of the entire solar energy input respectively. In SE module, the power output is 15.65 kW and corresponds to an overall efficiency of 36.45%.

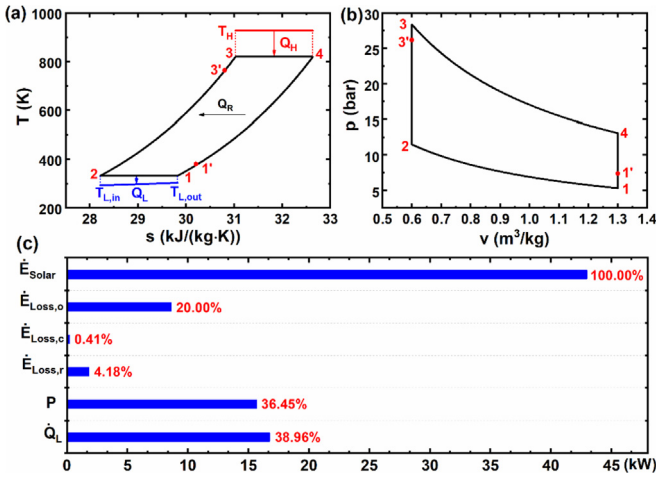

Fig. 4. T-s (a) p-v (b) diagrams and energy consumption distribution (c) of case study.

3.2. Sensitivity analysis

Sunshine illuminating on the concentrator varies continuously

Table 2
Results of case study.

$T_H(K)$	$T_h(K)$	$T_l(K)$	$T_{L,out}$(K)
927.21	819.25	331.87	303.16
$\dot{E}_{Solar}(kW)$	$\dot{E}_{Loss,o}(kW)$	$\dot{E}_{Loss,c}(kW)$	$\dot{E}_{Loss,r}(kW)$
42.95	8.59	0.18	1.80
$\dot{Q}_H(kW)$	$\dot{Q}_L(kW)$		$P(kW)$
32.39	−16.73		15.65
$\eta_{Receiver}(\%)$	$\eta_{SE}(\%)$		$\eta(\%)$
94.26	48.33		36.45

with meteorological condition. Thus, the influence of solar flux intensity and wind velocity on the system performance was investigated. In Fig. 5, solar flux intensity varies from 500 W/m^2 to 1000 W/m^2 and three wind velocity of 0, 6, 12 m/s are selected. Fig. 5-(a) indicates power output increases from 9 kW to around 23 kW linearly with the increase of I, and wind velocity reduces the power output. According to the corresponding hot end temperatures in Fig. 6-(a), it can be seen that receiver and gas in SE are both heated up significantly from 772 to 694 K to 1303 and 1164 K with the increase of I. Higher T_h not only corresponds to more heat absorbed by SE in Fig. 6-(c) according to Eq. (6), but also is beneficial for improving the thermal efficiency of internal Stirling cycle. Hence, the thermal efficiency of SE appears the trend of increasing from 43% to 56% as I gets stronger, then more power output is generated as well.

However, higher T_H also drives more heat to be lost into environment as depicted in Fig. 6-(b), then leads to the drop of receiver efficiency from 96% to 85%. As wind velocity increases to 12 m/s, receiver efficiency further drops by around 3.37% for wind aggravates convective heat loss coefficient. Thus, the deterioration of receiver efficiency leads the overall efficiency to increase with a decreasing slope and even appears slight drop with the increase of I. Namely, the overall efficiency tends to be relatively stable under high incident solar flux intensity in Fig. 5-(c), originating from the offset of heat engine efficiency increase and receiver efficiency decrease.

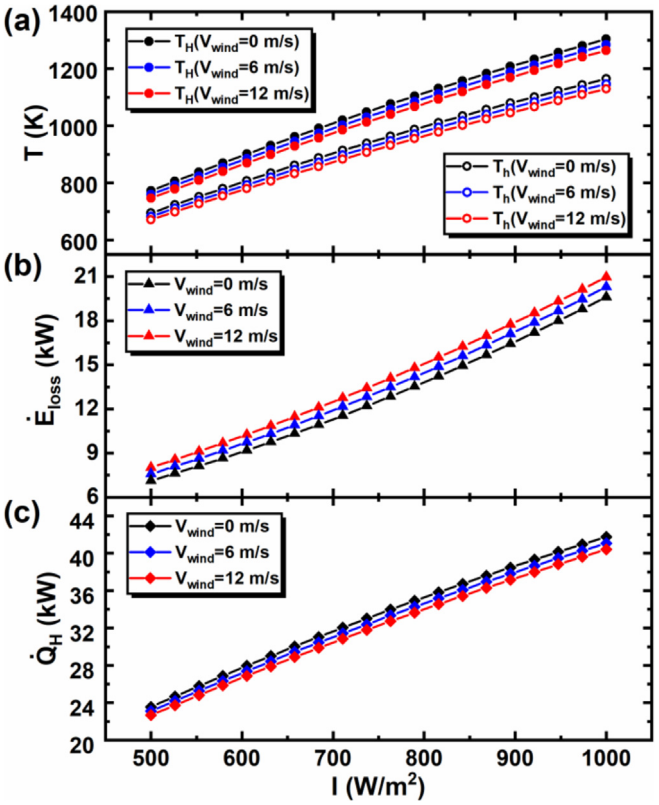

Fig. 6. Temperature of receiver and charged gas (a), energy loss (b) and absorbed heat by SE (c) as a function of solar flux intensity under different wind velocity.

As to the downstream SE subsystem, the variation of operational parameter influences the thermal requirement of SE. Consequentially, T_H varies to rebalance the energy conservation equation of

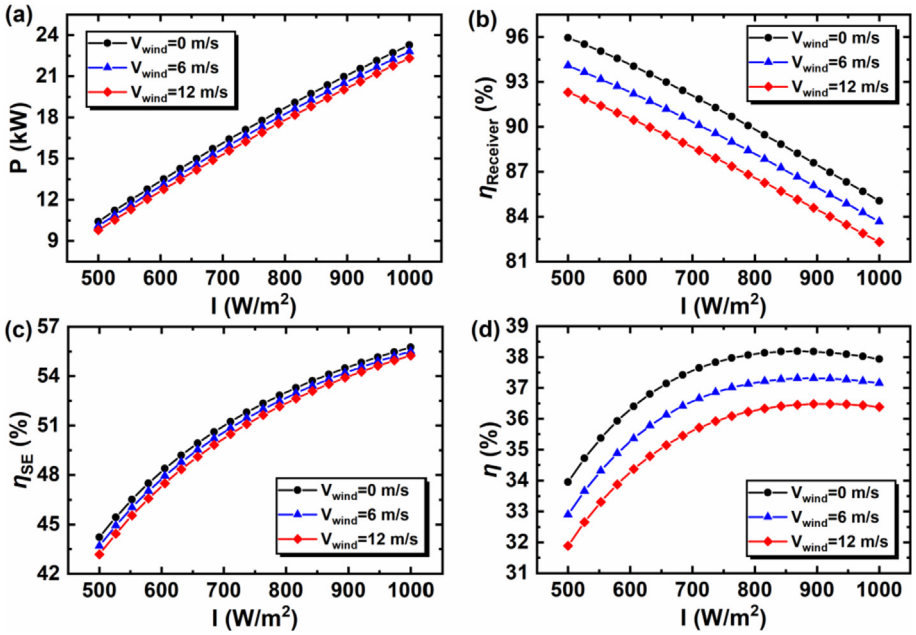

Fig. 5. System performance as a function of solar flux intensity under different wind velocity.

receiver under unsteady state in Eq. (21) until an updated steady state appears. It can be seen with a specified solar flux intensity, as $\dot{Q}_{H,Load}$ (thermal requirement of SE) increases instantaneously, the temperature of solar receiver will decrease to release the internal energy in the form of $m_R c_R \frac{dT_H}{dt}$. Meanwhile, the convective and radiative energy losses both drop simultaneously with the decrease of T_H to achieve the updated steady state.

$$m_R c_R \frac{dT_H}{dt} = IA_R C\eta_{optical} - h_c A_R (T_H - T_0) - \varepsilon\sigma A_R \left(T_H^4 - T_{sky}^4\right) - \dot{Q}_{H,Load} \tag{21}$$

Fig. 7 depicts the relationship of system performance with respect to m (charged gas mass) under different regenerator effectiveness. From Fig. 7-(a), it can be seen that with the increase of m, power output appears the trend of decreasing after increasing. Meanwhile, the increase of regenerator effectiveness from 0.7 to 0.9 improves the power output significantly. According to Eq. (6), the improvement of regenerator effectiveness is capable to reduce the thermal requirement of SE from solar receiver. Hence, higher T_H can be achieved in Fig. 8-(a) to emit more heat to environment and regulate the energy balance in receiver under the specified incident solar energy, which is depicted in Fig. 8-(b) and (c). Though heat absorbed by internal cycle drops slightly, thermal efficiency of heat engine gets improved with the increase of T_h. Hence, dish solar SE generates more shaft power with the improvement of regenerator effectiveness. As to the influence mechanism of m, Eq. (15) indicates power output is positively related to m. However, the increase of m also requires more heat for imperfect heat regeneration and isothermal expansion in Fig. 8-(c). With the aforementioned analysis, T_H will drop to meet the additional thermal requirement, and Fig. 8-(a) indeed indicates T_H and T_h both decline significantly with more gas charged into SE. According to Eq. (15), power output of dish solar SE is positively related to T_h as well. Hence, insufficient and excessive m of 0.2 and 1.2 g both generate low power output of 10.55 and 14.43 kW under regenerative effectiveness of 0.9. Namely, optimal m exits and corresponds to an appropriate heat absorbing temperature simultaneously to achieve the maximal power output.

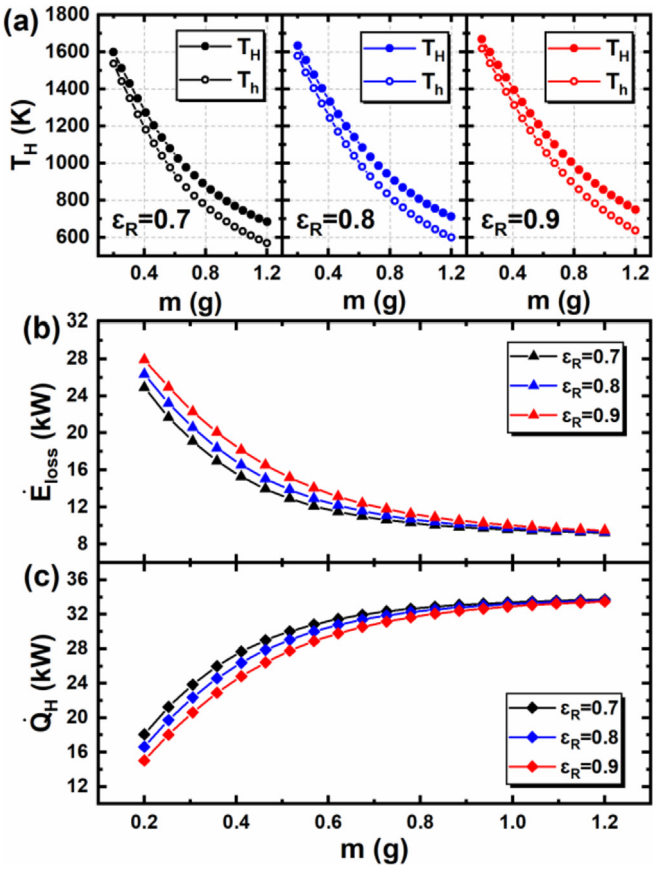

Fig. 8. Temperature of receiver and substance (a), energy loss (b) and absorbed heat by SE (c) as a function of charged gas mass in SE under different regenerator effectiveness.

Energy efficiency of each subsystems and overall system appear different trends with respect to m in Fig. 7-(b-d). Receiver efficiency

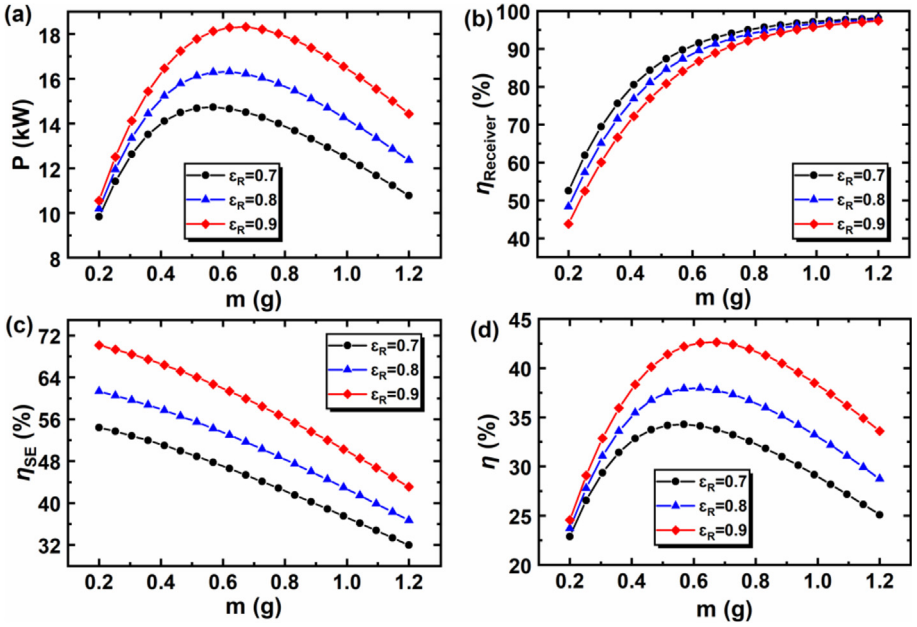

Fig. 7. System performance as a function of charged gas mass in SE under different regenerator effectiveness.

gets improved with more gas charged into SE from 50% to 90% under lower regenerative effectiveness, for low T_H reduces the heat loss of receiver then improves the efficiency. On the contrary, efficiency of SE drops by around 35% with the increase of m and deterioration of regenerative effectiveness, for it is positively related to T_h. In addition, with the incident solar energy specified, overall efficiency has the same trend with power output in Fig. 7-(d), it rises and falls in the range of 20–45%.

The sensitivity analysis indicates the variance of energy input and thermal load of SE both induce the variance of steady T_H, then influence the system performance drastically. In general, the system performance is positively related to I and optimal m exits for achieving the maximal power output and overall energy efficiency simultaneously. In order to further investigate the optimal system performance, optimization work was conducted.

3.3. Performance optimization

Common optimization methods mainly include analytical and numerical methods. With analytical method, the optimal results can be obtained directly with the derived equations under the optimal condition. However, as to some complex mathematical problems such as transcendental equation or equations with high order, the application of analytical optimization is limited. In comparison, numerical optimization method is capable to solve these problems for it only requires primitive function and tremendous repeated calculation procedure to search for the optimal value based on the fast calculation speed of computer. Various optimization algorithms were developed with different optimization paths as well. For implicit solutions exist in this mathematical model, three common numerical optimization algorithms of GA (genetic algorithm) [34], SA (simulated annealing) [35] and PSO (particle swarm optimization) [36] were employed to obtain the optimal m and ensure the accuracy of solutions. Table 3 lists the optimal results for cases those operate with different regenerative effectiveness.

It can be seen the results obtained by different algorithms are consistent under each regenerative effectiveness, while PSO requires the least time consumption. Optimal m of 0.56, 0.60 and 0.66 g are obtained to achieve the maximal power output of 14.73, 16.32 and 18.32 kW, and the corresponding maximal overall efficiencies are 34.29%, 37.99% and 42.65% respectively. With the improvement of regenerative effectiveness, the maximal power output increases by 3.6 kW and overall efficiency increases by 8.4%. Except for regenerator, the heat transfer ability of heater and cooler both influence the system performance as well for it decides the temperature level of external heat transfer process. Hence, the performance under different heater and cooler heat transfer ability is optimized as well and the results are listed in Tables 4 and 5.

Tables 4 and 5 both indicate the maximal power output and overall efficiency increase slightly with the improvement of heat transfer ability in heater and cooler. As K_H and K_L increase from 150 to 450 W/K and 250 to 750 W/K, maximal power output and overall efficiency get improved by around 1 kW and 3% respectively. The improvement of heat transfer ability in heater and cooler means heat can be transferred with less temperature difference. Namely, the charged gas can be heated to higher temperature during isothermal expanding and cooled down to lower temperature during isothermal compressing, which are listed in Tables 4 and 5 as well. According to Eq. (6), the increase of T_h and decrease of T_l are capable to enhance the thermal load of heat engine. In addition, higher upper temperature and lower bottom temperature achieve better thermal efficiency for the internal Stirling cycle. Hence, the double improvement of acquired utilizable heat and energy conversion efficiency generate more power output under better heat transfer ability of heater and cooler.

Table 3
Optimization results under different regenerative effectiveness.

ε_R	Algorithm	m_{Optimal}(g)	$P_{\max}$(kW)	η(%)	Time(s)
0.7	GA	0.56	14.73	34.29	7
	SA	0.56	14.73	34.29	5
	PSO	0.56	14.73	34.29	4
0.8	GA	0.60	16.32	37.99	6
	SA	0.60	16.32	37.99	5
	PSO	0.60	16.32	37.99	4
0.9	GA	0.66	18.32	42.65	6
	SA	0.66	18.32	42.65	5
	PSO	0.66	18.32	42.65	4

With a specified incident solar flux intensity, the maximal power output can be achieved by installing high performance heat exchangers and optimizing charged gas mass. Common power facilities are always optimized targeting with efficiency or power maximization [37,38], exergy destruction or entropy generation minimization [39,40] under steady operating condition. However, the most significant feature of dish solar SE is the dynamic power output driven by the fluctuating solar flux intensity. Thus, energy storage system such as battery is always integrated to store the fluctuating power in the day time and release stable power output as required. Consequentially, maximizing the daily generatable shaft work (integrating the production of power and time) should be considered as optimization target for a dish solar SE under daily dynamic condition.

In order to optimize m with a more rapid method, dish solar SE can be considered as operating steadily under the daily average solar flux intensity in Eq. (23). Thus, the optimization of m for maximizing daily generatable shaft work under dynamic condition can be simplified as the optimization of m for maximizing power output under steady daily average condition.

$$I(t) = -27.78t^2 + 666.67t - 3000 (t_1 = 7 \le t \le t_2 = 17) \quad (22)$$

$$\bar{I} = \frac{\int_{t_1}^{t_2} I(t)dt}{t_2 - t_1} \quad (23)$$

Considering solar flux intensity has a parabolic relationship with time in a day [6], and the maximal value appears at 12 h, the daily average intensity was obtained by Eq. (23) and equals to 768 W/m^2 as system operates from 7 h to 17 h in a day. Then the daily dynamic power output curve with the optimized m under $\bar{I}$ is plotted by black curve and compared with those under different optimized m from arbitrary I_{L} and I_{H} in Fig. 9 to indicate the maximal generatable shaft work in a day.

In Fig. 9-(a-1), the blue curve represents the daily power output which operates with the m optimized from low solar flux intensity I_L of 550 W/m^2. It can be seen the power output during 7–9 h and 15–17 h is similar with black curve but much lower during 9–15 h. This is because the optimal m obtained from I_L is less, then higher hot end temperatures can be achieved with strong incident sunshine, such as the temperature comparison between black and blue curves at 12 h in Fig. 9-(a-2). Though the thermal efficiency of SE gets enhanced, the drop of receiver efficiency is more significant under high temperature condition in Fig. 9-(a-3) and leads to the drop of overall efficiency consequentially. Meanwhile, the red curve in Fig. 9-(b-1) represents the daily power output which operates with the m optimized from high solar flux intensity I_H of 1150 W/m^2. The power output is similar during 10–14 h but weaker during 7–10 h and 14–17 h as compared with the black curve. For the

Table 4
Optimization results under different heat transfer ability of heater.

K_H(W/K)	$m_{Optimal}$(g)	P_{max}(kW)	η(%)	T_h(K)	$\dot{Q}_{H,Load}$(kW)	η_{SE}(%)
150	0.667	17.52	40.79	975	29.51	59.37
225	0.660	18.01	42.04	1002	30.07	60.05
300	0.656	18.32	42.65	1017	30.32	60.41
375	0.653	18.48	43.01	1026	30.47	60.64
450	0.651	18.58	43.25	1032	30.57	60.77

Table 5
Optimization results under different heat transfer ability of cooler.

K_L(W/K)	$m_{Optimal}$(g)	P_{max}(kW)	η(%)	T_l(K)	$\dot{Q}_{H,Load}$(kW)	η_{SE}(%)
250	0.624	17.73	41.23	345	29.82	59.45
375	0.645	18.12	42.19	329	30.16	60.09
500	0.656	18.32	42.65	321	30.32	60.41
625	0.662	18.44	42.92	316	30.42	60.60
750	0.667	18.51	43.10	313	30.49	60.73

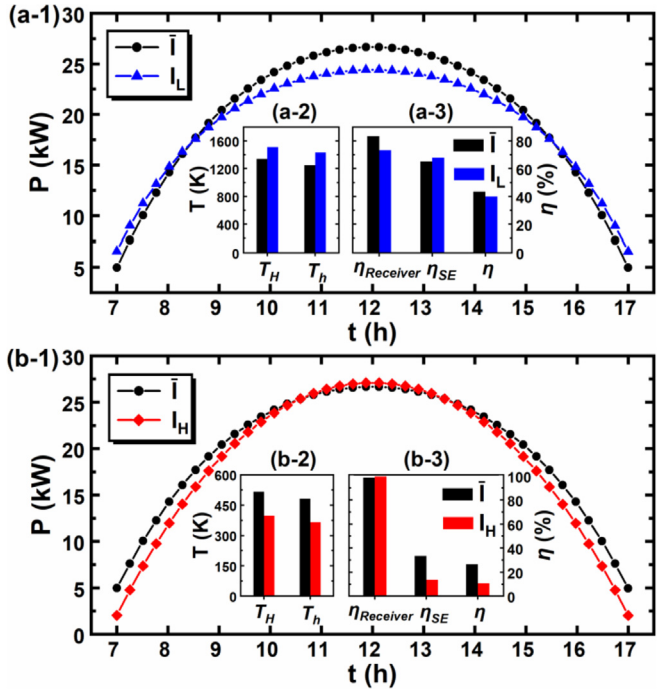

Fig. 9. Daily dynamic power output comparison under different optimized m.

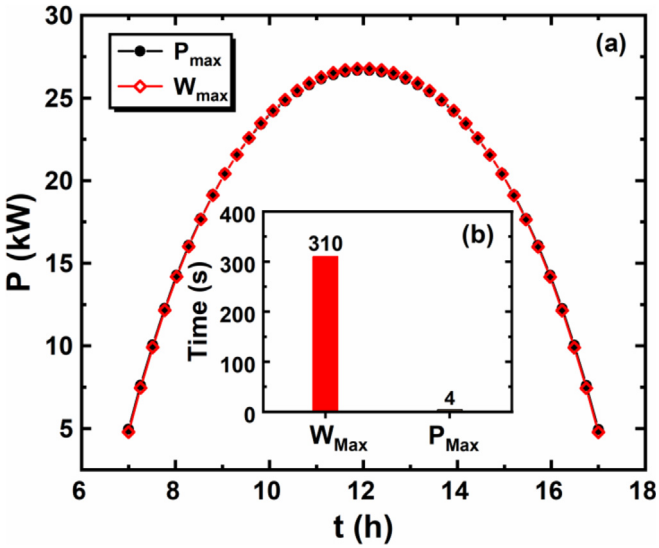

Fig. 10. Daily dynamic power output comparison with different optimization strategies.

optimal m obtained from I_H is larger, weak incident solar flux during 7–10 h and 14–17 h is insufficient to heat the receiver and gas to high temperature. The temperature and efficiency between red and black curves at 7 h are compared in Fig. 9-(b-2) and 9-(b-3) as well. It can be seen efficiency of receiver in red is more efficient but extremely slightly, while the much lower thermal efficiency of SE under middle temperature condition induces more inefficient overall performance. Hence, m optimized under $\bar{I}$ achieves better daily dynamic performance for it corresponds to larger area beneath the dynamic power curve (daily generatable shaft work) in Fig. 9-(a-1) and Fig. 9-(b-1).

For further testifying the power output curve obtained from the steady optimization strategy, it is compared with optimal power output curve in red which is obtained from the optimized m targeting with maximal daily work in Fig. 10. It can be seen the curves coincide with each other and the integrated daily work are 726.82 and 727.02 MJ respectively. However, the time cost for computation in Fig. 10-(b) indicates the steady optimization strategy consumes much less computation. Thus, the steady optimization of m for maximizing power output under daily average condition is a feasible and more rapid strategy to obtain the optimal daily dynamic system performance.

Based on the heat exchangers with high performance and optimized m, the daily dynamic theoretical performance is plotted in Fig. 11. Wind with high velocity reduces the performance of sub and overall systems in some extent. Power output rises and drops in the range of 5 and 26 kW, while the receiver efficiency drops and rises in the range of 98% and 81% during a day. As to the efficiency of SE and overall system, the minimal values of 32% and 24% appear at 7 and 17 h, the maximal values of 62% and 44% are relatively stable in the time duration between 9 and 15 h.

4. Conclusion

With the modified theoretical thermally irreversible model of dish solar SE system and corresponding algorithm, the direct influence of solar flux intensity and wind velocity on the system performance was analyzed. In general, the system performance is

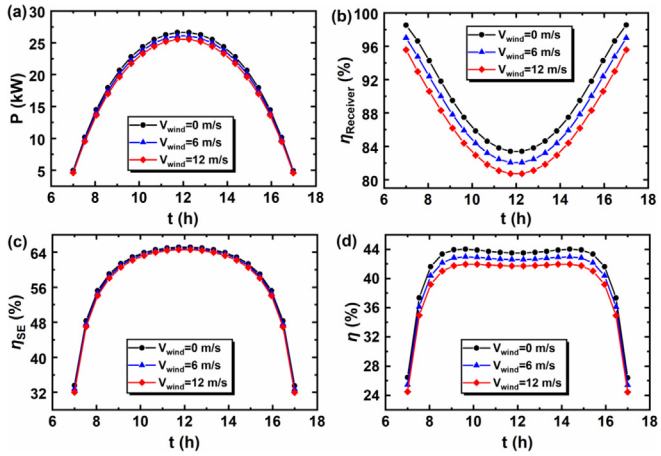

Fig. 11. Daily dynamic theoretical performance under different wind velocity.

positively related to solar flux intensity, while wind aggravates the convective heat loss then deteriorates the system performance. Results indicate that receiver temperature gets elevated with the increase of incident solar flux intensity to improve the heat transferred into SE module and thermal efficiency, though heat dissipation into environment increases for achieving the energy balance at hot end as well. The variance of SE thermal requirement originating from the change of charged gas mass also influences the energy balance of receiver. The harmonization point of positive influence originated from the increase of gas mass and the negative influence originated from the accompanying decrease of heat absorbing temperature, an optimal charged gas mass exists for achieving the maximal power output. Better thermal performance of heater, regenerator and cooler are capable to improve the overall performance for higher upper and lower bottom temperatures of internal cycle can be achieved. In order to obtain the maximal generatable shaft work in a day using less computation, gas mass should be optimized under the daily average solar flux intensity. With the optimized gas mass and more efficient heat exchangers, maximal theoretical peak power output of 25 kW and overall efficiency of 44% are obtained.

Acknowledgements

We acknowledge the support received from the National Natural Science Foundation of China (51736004, 51706076).

Appendix

This model is compared with a previously reported experiment in Table A1. It can be seen the model overestimated the real performance of dish solar Stirling engine for some precise geometry related losses were neglected for simplicity.

Table A1
Comparison between model and previously reported experiment

	$\dot{E}_{Solar}$(kW)	$\dot{Q}_H$(kW)	P(kW)	η(%)
Theoretical model	48.02	33.42	15.76	32.82
Experiment [41]	48.02	31.63	12.25	25.51

However, the energy distribution in Table A1 are basically approximate and the results in this work can be reasonably explained with current relative theory. As to the fundamental thermodynamic analysis and optimization, the results obtained by the model have some qualitative significance within the theoretical scope.

Nomenclature

A_R	**Solar receiver area** m^2
$c_{p,w}$	Specific heat at constant pressure of coolant $J/(kg \cdot K)$
c_R	Specific heat of solar receiver $J/(kg \cdot K)$
c_v	Specific heat at constant volume of gas $J/(kg \cdot K)$
C	Concentration ratio
F	Rotating frequency of Stirling engine shaft Hz
h_c	Convective heat transfer coefficient of solar receiver W $/(m^2 \cdot$K)
I	Incident solar flux intensity W $/m^2$
K_H	Heat transfer ability at hot end W/K
K_L	Heat transfer ability at cold end W/K
m	Mass of charged gas kg
m_R	Mass of solar receiver kg
$\dot{m}_w$	Mass flow rate of coolant kg/s
p	Pressure of charged gas Pa
P	Power output W
Q_{12}	Cyclic heat released under isothermal compression J
Q_{23}	Cyclic heat absorbed under isochoric heating J
Q_{34}	Cyclic heat absorbed under isothermal expansion J
Q_{41}	Cyclic heat released under isochoric cooling J
Q_H	Cyclic heat absorbed from heat source J
Q_L	Cyclic heat released to heat sink J
$\dot{Q}_{H,Supplement}$	Heat released per second by receiver at hot end W
$\dot{Q}_{H,Transfer}$	Heat transferred per second at hot end W
$\dot{Q}_{H,Load}$	Heat absorbed per second by gas at hot end W
$\dot{Q}_{L,Supplement}$	Heat released per second by gas at cold end W
$\dot{Q}_{L,Transfer}$	Heat transferred per second at cold end W
$\dot{Q}_{L,Load}$	Heat absorbed per second by coolant at cold end W
R_g	Gas constant $J/(kg \cdot K)$
t	Time s
T_0	Ambient temperature K
T_h	Heat absorbing temperature of charged gas K
T_l	Heat releasing temperature of charged gas K
T_{sky}	Temperature of sky K
T_H	Temperature of solar receiver K
$T_{L,in}$	Inlet temperature of coolant K
$T_{L,out}$	Outlet temperature of coolant K
v	Specific volume m^3/kg
V_{wind}	Wind of velocity m/s

Greek Symbols

δ	Relative error
ε	Emissivity of solar receiver
ε_R	Regenerator effectiveness
$\eta_{optical}$	Optical efficiency %
$\eta_{Receiver}$	Efficiency of solar receiver %
η_{SE}	Efficiency of Stirling engine %
η	Efficiency of dish solar Stirling engine %
σ	Stefan Boltzmann constant $W/(m^2 \cdot K^4)$

Subscripts

1–4	State turning points
w	Water
H	Hot end
L	Cold end
R	Solar receiver

Abbreviations

GA	Genetic algorithm
LINMAP	Linear programming techniques for multidimensional analysis of preference
NSGA-II	Non-dominated sorted genetic algorithm-II
PSO	Particle swarm optimization
SA	Simulated annealing
SE	Stirling engine
SQP	Sequential quadratic programming
TOPSIS	Technique for order preference by similarity to an ideal solution

References

[1] Shaulsky E, Boo C, Lin S, Elimelech M. Membrane-based osmotic heat engine with organic solvent for enhanced power generation from low-grade heat. Environ Sci Technol 2015;49(9):5820–7.
[2] Schiro F, Benato A, Stoppato A, Destro N. Improving photovoltaics efficiency by water cooling: modelling and experimental approach. Energy 2017;137:798–810.
[3] Hussain T, Islam MD, Kubo I, Watanabe T. Study of heat transfer through a cavity receiver for a solar powered advanced Stirling engine generator. Appl Therm Eng 2016;104:751–7.
[4] Luo H, Wang R, Dai Y. The effects of operation parameter on the performance of a solar-powered adsorption chiller. Appl Energy 2010;87(10):3018–22.
[5] Pouyfaucon AB, García-Rodríguez L. Solar thermal-powered desalination: a viable solution for a potential market. Desalination 2018;435:60–9.
[6] Long R, Li B, Liu Z, Liu W. Performance analysis of a solar-powered solid state heat engine for electricity generation. Energy 2015;93:165–72.
[7] Mancini T, Heller P, Butler B, Osborn B, Schiel W, Goldberg V, et al. Dish-Stirling systems: an overview of development and status. J Sol Energy Eng 2003;125(2):135–51.
[8] Çınar C, Aksoy F, Solmaz H, Yılmaz E, Uyumaz A. Manufacturing and testing of an α-type Stirling engine. Appl Therm Eng 2018;130:1373–9.
[9] Xin F, Liu Z, Wang S, Liu W. Study of heat transfer in oscillatory flow for a Stirling engine heating tube inserted with spiral spring. Appl Therm Eng 2018;143:182–92.
[10] Cheng C-H, Yang H-S. Theoretical model for predicting thermodynamic behavior of thermal-lag Stirling engine. Energy 2013;49:218–28.
[11] Cheng C-H, Chen Y-F. Numerical simulation of thermal and flow fields inside a 1-kW beta-type Stirling engine. Appl Therm Eng 2017;121:554–61.
[12] Lai X, Long R, Liu Z, Liu W. Stirling engine powered reverse osmosis for brackish water desalination to utilize moderate temperature heat. Energy 2018;165:916–30.
[13] Hafez AZ, Soliman A, El-Metwally KA, Ismail IM. Design analysis factors and specifications of solar dish technologies for different systems and applications. Renew Sustain Energy Rev 2017;67:1019–36.
[14] Aksoy F, Karabulut H. Performance testing of a Fresnel/Stirling micro solar energy conversion system. Energy Convers Manag 2013;75:629–34.
[15] Mendoza Castellanos LS, Carrillo Caballero GE, Melian Cobas VR, Silva Lora EE, Martinez Reyes AM. Mathematical modeling of the geometrical sizing and thermal performance of a Dish/Stirling system for power generation. Renew Energy 2017;107:23–35.
[16] Aksoy F, Karabulut H, Çınar C, Solmaz H, Özgören YÖ, Uyumaz A. Thermal performance of a Stirling engine powered by a solar simulator. Appl Therm Eng 2015;86:161–7.
[17] Ferreira AC, Teixeira S, Teixeira JC, Martins LB. Design optimization of a solar dish collector for its application with stirling engines. 2015 (57434): V06AT7A033.
[18] Ferreira AC, Nunes ML, Teixeira JCF, Martins LASB, Teixeira SFCF, Nebra SA. Design of a solar dish Stirling cogeneration system: application of a multi-objective optimization approach. Appl Therm Eng 2017;123:646–57.
[19] Ferreira AC, Nunes ML, Teixeira JCF, Martins LASB, Teixeira SFCF. Thermodynamic and economic optimization of a solar-powered Stirling engine for micro-cogeneration purposes. Energy 2016;111:1–17.
[20] Bădescu V. Optimum operation of a solar converter in combination with a Stirling or Ericsson heat engine. Energy 1992;17(6):601–7.
[21] Blank DA, Wu C. Power optimization of an extra-terrestrial, solar-radiant stirling heat engine. Energy 1995;20(6):523–30.
[22] Kaushik SC, Kumar S. Finite time thermodynamic analysis of endoreversible Stirling heat engine with regenerative losses. Energy 2000;25(10):989–1003.
[23] Chen J, Yan Z, Chen L, Andresen B. Efficiency bound of a solar-driven stirling heat engine system. Int J Energy Res 1998;22(9):805–12.
[24] Liao T, Lin J. Optimum performance characteristics of a solar-driven Stirling heat engine system. Energy Convers Manag 2015;97:20–5.
[25] Ahmadi MH, Ahmadi MA, Mellit A, Pourfayaz F, Feidt M. Thermodynamic analysis and multi objective optimization of performance of solar dish Stirling engine by the centrality of entransy and entropy generation. Int J Electr Power Energy Syst 2016;78:88–95.
[26] Ahmadi MH, Mohammadi AH, Dehghani S, Barranco-Jiménez MA. Multi-objective thermodynamic-based optimization of output power of Solar Dish-Stirling engine by implementing an evolutionary algorithm. Energy Convers Manag 2013;75:438–45.
[27] Ahmadi MH, Sayyaadi H, Dehghani S, Hosseinzade H. Designing a solar powered Stirling heat engine based on multiple criteria: maximized thermal efficiency and power. Energy Convers Manag 2013;75:282–91.
[28] Yaqi L, Yaling H, Weiwei W. Optimization of solar-powered Stirling heat engine with finite-time thermodynamics. Renew Energy 2011;36(1):421–7.
[29] Costea M, Petrescu S, Harman C. The effect of irreversibilities on solar Stirling engine cycle performance. Energy Convers Manag 1999;40(15):1723–31.
[30] Al-Dafaie AMA, Dahdolan Md-E, Al-Nimr MdA. Utilizing the heat rejected from a solar dish Stirling engine in potable water production. Sol Energy 2016;136:317–26.
[31] Urieli I, Berchowitz DM. Stirling cycle engine analysis: A. Hilger Bristol; 1984.
[32] Liu W, Liu P, Dong ZM, Yang K, Liu ZC. A study on the multi-field synergy principle of convective heat and mass transfer enhancement. Int J Heat Mass Transf 2019;134:722–34.
[33] Qiu Y, Li M-J, Wang W-Q, Du B-C, Wang K. An experimental study on the heat transfer performance of a prototype molten-salt rod baffle heat exchanger for concentrated solar power. Energy 2018;156:63–72.
[34] Long R, Li B, Liu Z, Liu W. Performance analysis of reverse electrodialysis stacks: channel geometry and flow rate optimization. Energy 2018;158:427–36.
[35] Kirkpatrick S, Gelatt CD, Vecchi MP. Optimization by simulated annealing. Science 1983;220(4598):671–80.
[36] Kennedy J. Particle swarm optimization. Encyclopedia of machine learning 2010:760–6.
[37] Singh S, Agrawal S. Efficiency maximization and performance evaluation of hybrid dual channel semitransparent photovoltaic thermal module using fuzzyfied genetic algorithm. Energy Convers Manag 2016;122:449–61.
[38] Wu S-j, Wang S, Yang C-j, Xie K-r. Energy management for thermoelectric generators based on maximum power point and load power tracking. Energy Convers Manag 2018;177:55–63.
[39] Liu W, Liu P, Wang JB, Zheng NB, Liu ZC. Exergy destruction minimization: a principle to convective heat transfer enhancement. Int J Heat Mass Transf 2018;122:11–21.
[40] Cheng X, Liang X. Discussion on the applicability of entropy generation minimization to the analyses and optimizations of thermodynamic processes. Energy Convers Manag 2013;73:121–7.
[41] Reinalter W, Ulmer S, Heller P, Rauch T, Gineste J-M, Ferriere A, et al. Detailed performance analysis of a 10kW Dish/ stirling system. J Sol Energy Eng 2008;130(1):011013.